Journal of Biomolecular NMR, **17:** 239–255, 2000.
KLUWER/ESCOM

Backbone dynamics of a bacterially expressed peptide from the receptor binding domain of *Pseudomonas aeruginosa* pilin strain PAK from heteronuclear ^{1}H-^{15}N NMR spectroscopy

A. Patricia Campbell[a,*], Leo Spyracopoulos[b], Randall T. Irvin[c,d] & Brian D. Sykes[b,d]
[a]*Department of Medicinal Chemistry, School of Pharmacy, University of Washington, Seattle, WA 98195, U.S.A.;*
[b]*Department of Biochemistry, and* [c]*Department of Medical Microbiology and Immunology, University of Alberta, Edmonton, AB, Canada T6G 2H7;*
[d]*Protein Engineering Network of Centers of Excellence, University of Alberta, Edmonton, AB, Canada T6G 2S2*

Received 23 February 2000; Accepted 3 May 2000

Key words: backbone dynamics, pilin, ^{15}N NMR relaxation, *Pseudomonas aeruginosa*, recombinant peptide

Abstract

The backbone dynamics of a ^{15}N-labeled recombinant PAK pilin peptide spanning residues 128–144 in the C-terminal receptor binding domain of *Pseudomonas aeruginosa* pilin protein strain PAK (Lys^{128}-Cys-Thr-Ser-Asp-Gln-Asp-Glu-Gln-Phe-Ile-Pro-Lys-Gly-Cys-Ser-Lys^{144}) were probed by measurements of ^{15}N NMR relaxation. This PAK(128–144) sequence is a target for the design of a synthetic peptide vaccine effective against multiple strains of *P. aeruginosa* infection. The ^{15}N longitudinal (T_1) and transverse (T_2) relaxation rates and the steady-state heteronuclear {^{1}H}-^{15}N NOE were measured at three fields (7.04, 11.74 and 14.1 Tesla), five temperatures (5, 10, 15, 20, and 25 °C) and at pH 4.5 and 7.2. Relaxation data was analyzed using both the 'model-free' formalism [Lipari, G. and Szabo, A. (1982) *J. Am. Chem. Soc.*, **104**, 4546–4559 and 4559–4570] and the reduced spectral density mapping approach [Farrow, N.A., Szabo, A., Torchia, D.A. and Kay, L.E. (1995) *J. Biomol. NMR*, **6**, 153–162]. The relaxation data, spectral densities and order parameters suggest that the type I and type II β-turns spanning residues Asp^{134}-Glu-Gln-Phe^{137} and Pro^{139}-Lys-Gly-Cys^{142}, respectively, are the most ordered and structured regions of the peptide. The biological implications of these results will be discussed in relation to the role that backbone motions play in PAK pilin peptide immunogenicity, and within the framework of developing a pilin peptide vaccine capable of conferring broad immunity across *P. aeruginosa* strains.

Abbreviations: DSS, 2,2-dimethyl-2-sila-5-pentanesulfonate; Hs, homoserine; NOE, nuclear Overhauser effect.

Introduction

Peptide backbone motions play an important role in two dynamically driven processes: the recognition and docking of biologically active peptides to their receptor proteins, and the folding of the nascent polypeptide chain into its final folded state. The importance of peptide backbone dynamics in protein folding and receptor recognition is reflected in the number of studies of peptide dynamics in the last few years (Dellwo and Wand, 1989; Hu et al., 1990; Palmer et al., 1991, 1993; Palmer and Case, 1992; Blackledge et al., 1993; Chen et al., 1993; Fan et al., 1993; Fan and Mayo, 1995; Briand and Kopple, 1995; Friedrichs et al., 1995; Jarvis and Craik, 1995; Spyracopoulos et al., 1996; Daragan et al., 1997; Kemple et al., 1997; Alexandrescu et al., 1998).

Recently developed solution NMR methods for measuring ^{13}C and ^{15}N relaxation have permitted the characterization of backbone and side-chain motional properties of peptides on the pico- to millisecond time scale. These motional studies have largely involved natural abundance ^{13}C NMR relaxation measurements

*To whom correspondence should be addressed. E-mail: apc@u.washington.edu

(Briand and Kopple, 1995; Friedrichs et al., 1995; Jarvis and Craik, 1995; Mikhailov et al., 1996; Lu and Van Halbeek, 1997). However, isotopic enrichment at selected residues in peptides during solid-state synthesis has also been used to generate samples for both ^{13}C (Daragan et al., 1997; Kemple et al., 1997) and ^{15}N (Chen et al., 1993; Fan et al., 1993) NMR relaxation measurements. ^{15}N and/or ^{13}C relaxation studies of peptides enriched isotopically by biosynthetic means are not common (Spyracopoulos et al., 1996; Alexandrescu et al., 1998). This is due in part to difficulties associated with expression and purification of small peptides in bacterial systems.

The small number of ^{15}N NMR relaxation studies of peptides compared to similar studies of proteins may also arise from difficulties inherent in choosing the proper motional models with which to interpret peptide relaxation data. Generally, peptides of about 20 residues or less are flexible in solution at temperatures of approximately 30 °C and are not expected to possess substantial secondary structure in comparison to a folded protein. Peptide relaxation data has been interpreted using models for molecular diffusion (Mikhailov et al., 1996), and the 'wobbling in a cone' model (Jarvis and Craik, 1995). For proteins, the model-free formalism developed by Lipari and Szabo (1982a,b) is widely used for the analysis of backbone dynamics data (Palmer, 1993, 1997; Wagner, 1993; Kay, 1998; Roberts, 1999). The application of the model-free approach to flexible peptides is not straightforward, as the analysis is generally valid only for molecules whose overall rotational correlation time is longer than about 2–4 ns. In addition, the overall rotation of the molecule should dominate backbone relaxation in comparison to internal motions, whose contribution to relaxation is required to be significantly smaller. Peptides in solution may experience multiple motions, perhaps with similar time scales. Consequently, the general conditions outlined above are not adequately satisfied. A recent approach for the analysis of the dynamics of proteins is the method of spectral density mapping (Peng and Wagner, 1992a,b). The attractiveness of the spectral density mapping approach is due in part to the fact that the method does not make assumptions about the motions of a molecule. In this regard, the method should be ideally suited to the analysis of peptide backbone relaxation data.

Recently, we produced a uniformly ^{15}N-labeled immunogenic peptide spanning residues 128–144 in the C-terminal receptor binding domain of *Pseudomonas aeruginosa* pilin protein strain PAK (Lys^{128}-Cys-Thr-Ser-Asp-Gln-Asp-Glu-Gln-Phe-Ile-Pro-Lys-Gly-Cys-Ser-Lys^{144}) using a bacterial expression system (Campbell et al., 1997a). The PAK(128–144) sequence is the target for the design of a synthetic peptide vaccine effective against multiple strains of *P. aeruginosa* infection. The oxidized form of the recombinant PAK pilin peptide (containing the intramolecular disulfide bridge Cys^{129}—Cys^{142}) undergoes *cis/trans* isomerization of the central Ile^{138}-Pro^{139} peptide bond. The *cis/trans* isomerization is manifested as a doubling of ^1H NMR resonances with a *trans*:*cis* ratio of 4:1 at 5 °C (McInnes et al., 1994). Structural studies using multinuclear, multidimensional NMR spectroscopy have shown the *trans* isomer to be disordered at its N- and C-termini and ordered within the central region that encompasses two β-turns. One turn is a type I β-turn spanning residues Asp^{134}-Glu-Gln-Phe^{137}, and the other is a type II β-turn, spanning residues Pro^{139}-Lys-Gly-Cys^{142} (Campbell et al., 1997a).

In this study we undertake an analysis of backbone amide ^{15}N NMR relaxation measurements of the *trans* isomer of the ^{15}N-labeled recombinant PAK pilin peptide to further the understanding of the structural and dynamic determinants of immunogenicity of the free peptide. The results are discussed within the framework of developing a pilin peptide vaccine capable of conferring broad immunity across multiple *P. aeruginosa* strains.

Materials and methods

Preparation of recombinant ^{15}N-labeled PAK pilin peptide NMR sample

Details of the vector construction, cloning, expression and purification of the ^{15}N-labeled PAK 128–144(Hs145) pilin peptide have been previously described in detail (Tripet et al., 1996; Campbell et al., 1997a). The NMR sample was prepared by dissolving the recombinant ^{15}N-labeled PAK pilin peptide in 500 μl of 90% H_2O/10% D_2O PBS buffer to a concentration of 1 mM. DSS was added as an internal chemical shift reference and the final pH was 4.5.

Relaxation measurements

^{15}N NMR relaxation measurements were performed at a temperature of 5 °C, and three magnetic field strengths: 7.04 (300 MHz ^1H frequency), 11.74 (500 MHz ^1H frequency), and 14.1 Tesla (600 MHz

^{1}H frequency). Additional ^{15}N NMR relaxation measurements were made at 11.74 Tesla and 10, 15, 20, and 25 °C. Spectra were acquired with Varian Unity (300 and 600 MHz) and Varian Inova (500 MHz) NMR spectrometers. The 500 and 600 MHz spectrometers were equipped with triple resonance probes containing actively shielded *z*-gradients. The 300 MHz spectrometer was equipped with a double resonance, inverse broadband probe, with the outer coil tuned to ^{15}N.

Pulse sequences used to record ^{15}N-T_1 and T_2 values and the steady-state heteronuclear {^{1}H}-^{15}N NOE at 500 and 600 MHz were from Farrow et al. (1994). Relaxation delays of 11.1, 22.2, 44.4, 88.8, 177.6, 355.2, 710.4, 1420.8 ms (T_1^{500}); 15.6, 31.3, 46.9, 62.6, 93.4, 109.2, 124.8, 140.4, 156.4, 171.8, 187.2 ms (T_2^{500}); 11.1, 22.2, 44.4, 88.8, 177.6, 355.2, 710.4, 1420.8 ms (T_1^{600}); and 16.3, 32.6, 48.9, 65.2, 81.4, 97.8, 114.0, 130.4, 146.9, 163.3, 179.3 ms (T_2^{600}) were used. Field strengths of 6.5, 3.8, 5.3, and 4.3 kHz were used for ^{15}N excitation pulses in the T_1^{500}, T_2^{500}, T_1^{600} and T_2^{600} experiments, respectively. WALTZ-16 decoupling (Shaka et al., 1983) of ^{15}N during acquisition was performed using field strengths of 1.2 and 0.8 kHz for the 500 and 600 MHz data, respectively. Delays between transients of 1.2 s were employed in the measurement of T_1^{500} and T_1^{600} values, whereas delays of 2.0 s were employed in the measurement of T_2^{500} and T_2^{600} values. All T_1 and T_2 experiments were obtained with 32 transients per complex point. The {^{1}H}-^{15}N steady-state NOE was obtained at 500 and 600 MHz by recording spectra with and without 3.0 s of ^{1}H saturation. In the case of spectra acquired without NOE, a net relaxation delay of 5.0 s was employed, whereas a delay of 2.0 s prior to 3.0 s of ^{1}H saturation was employed for spectra with NOE. The NOE^{500} experiment used a field of 6.5 kHz for ^{15}N excitation pulses, 1.2 kHz for WALTZ-16 decoupling, and 10.6 kHz for ^{1}H saturation. The NOE^{600} experiment used a field of 5.3 kHz for ^{15}N excitation pulses, 0.8 kHz for WALTZ-16 decoupling, and 10.4 kHz for ^{1}H saturation. The NOE^{500} and NOE^{600} experiments were obtained with 64 transients per complex point. The spectral width used for all 500 MHz experiments was 6000 and 970 Hz for ^{1}H and ^{15}N, respectively. The spectral width used for all 600 MHz experiments was 7000 and 1220 Hz for ^{1}H and ^{15}N, respectively.

The pulse sequences used to record ^{15}N-T_1 and T_2 values and the {^{1}H}-^{15}N NOE at 300 MHz were modified sequences taken from Barbato et al. (1992). Relaxation delays of 12, 40, 152, 292, 572, 972 ms, and 0.0, 8.3, 16.6, 41.4, 66.2, 99.3, 165.5, 330.8 ms were used for the T_1^{300} and T_2^{300} experiments, respectively. Field strengths of 3.7 kHz were used for the ^{15}N excitation pulses in the T_1^{300} and T_2^{300} experiments. Delays of 3.0 s between transients were employed in the measurement of T_1^{300} and T_2^{300} values. All T_1 and T_2 experiments were obtained with 128 transients per complex point. The {^{1}H}-^{15}N steady-state NOE values were obtained at 300 MHz as described above, but using a pulse sequence modified from Barbato et al. (1992) to include weak ^{1}H saturation for water suppression. The NOE^{300} experiment used a field of 3.7 kHz for ^{15}N excitation pulses, 0.6 kHz for WALTZ-16 decoupling, 13.5 kHz for ^{1}H saturation, and 128 transients per complex point. The spectral widths used for all 300 MHz experiments were 4000 Hz for ^{1}H and 660 Hz for ^{15}N.

Data processing and analysis

All 2D data sets were processed on SUN Sparc5 and Silicon Graphics Indigo2 workstations using the NMRPipe software (Delaglio et al., 1995). Assignment of NMR spectra was achieved with the program PIPP (Garrett et al., 1991). Typically, spectra were processed in the acquisition and indirect dimensions with 90° shifted sine-bell squared window functions. T_1 and T_2 values were determined by non-linear least-squares fitting of the measured peak heights to a two-parameter exponential decay. Fitting was accomplished with the xcrvfit program (executable available at the following address: http://www.pence.ualberta.ca/∼rbo/xcrvfit). Uncertainties in T_1 and T_2 values were approximated from the non-linear least-squares fits. The steady-state NOE values were determined from the ratio of the peak intensities obtained with and without ^{1}H saturation.

Results

Assignment of ^{15}N-labeled recombinant PAK(128–144) pilin peptide

The ^{1}H and ^{15}N resonances of the NMR spectrum of the uniformly ^{15}N-labeled recombinant PAK(128–144) pilin peptide were previously assigned at pH 5.0 and at 5 and 25 °C (Campbell et al., 1995, 1997a). The ^{1}H and ^{15}N chemical shifts at 10, 15, and 20 °C (pH 4.5) were assigned by following the temperature

dependence of cross peaks in the 2D ^{1}H-^{15}N HSQC NMR spectra of the recombinant peptide.

Temperature dependence of the ^{15}N-T_1 and T_2, and {^{1}H}-^{15}N NOE

^{15}N-T_1 and T_2 relaxation times and the {^{1}H}-^{15}N NOE at 500 MHz were measured for the recombinant PAK pilin peptide at pH 4.5, and at 5, 10, 15, 20, and 25 °C. The T_1 and T_2 values are available as Supplementary material (Table S1, to be obtained from the authors on request) and are shown in Figure 1. At 5 °C, T_1 times of 536 ± 3 and 685 ± 6 ms, observed for Lys^{144} and Hs^{145}, respectively, are longer than the average value of 471 ms. T_2 times of 567 and 751 ms for Lys^{144} and Hs^{145}, respectively, are significantly longer than the average value of 360 ms. Additionally, {^{1}H}-^{15}N NOE values of −0.23 ± 0.01 and −0.51 ± 0.01 for Lys^{144} and Hs^{145}, respectively, are significantly more negative than the average value of +0.1. These T_1, T_2 and {^{1}H}-^{15}N NOE values indicate that Lys^{144} and Hs^{145} are the most flexible residues within the peptide at 5 °C, and further suggest that the disulfide bridge (Cys^{129}—Cys^{142}) restricts the internal mobility of residues within the cyclic portion of the peptide (129–143). Within the disulfide loop region, the T_2 times at 5 °C are the shortest for Thr^{130}, Phe^{137}, Ile^{138} and Lys^{140}, suggesting a further restriction on mobility or a shortening of T_2 due to conformational exchange phenomena.

The effect of increasing temperature on the backbone dynamics of the PAK pilin peptide is generally observed as increases in ^{15}N-T_1 and T_2 relaxation times, and decreases in {^{1}H}-^{15}N NOE values (Figure 1). For example, the average T_1 for all residues within the loop region (129–142) is 450 ± 20 ms at 5 °C, 480 ± 20 ms at 10 °C, 570 ± 20 ms at 15 °C, 650 ± 40 ms at 20 °C, and 660 ± 20 ms at 25 °C. The increases in T_1 and T_2 with temperature indicate that the peptide is experiencing more rapid molecular rotation at higher temperatures. This is expected from Stokes' law, $\tau_c = V\eta/(k_BT)$, in which τ_c is the rotational correlation time, V is the hydrated volume of the molecule, η is the solvent viscosity, and T is the temperature.

In general, T_2 times for most residues in the PAK pilin peptide also increase with temperature. However, increases are not uniform across the sequence, as seen for T_1 (Figure 1). For example, T_2 times of Lys^{140} increase substantially with temperature, T_2 times of Hs^{145} remain fairly constant with temperature, and the T_2 times of Cys^{129} decrease substantially with tem-

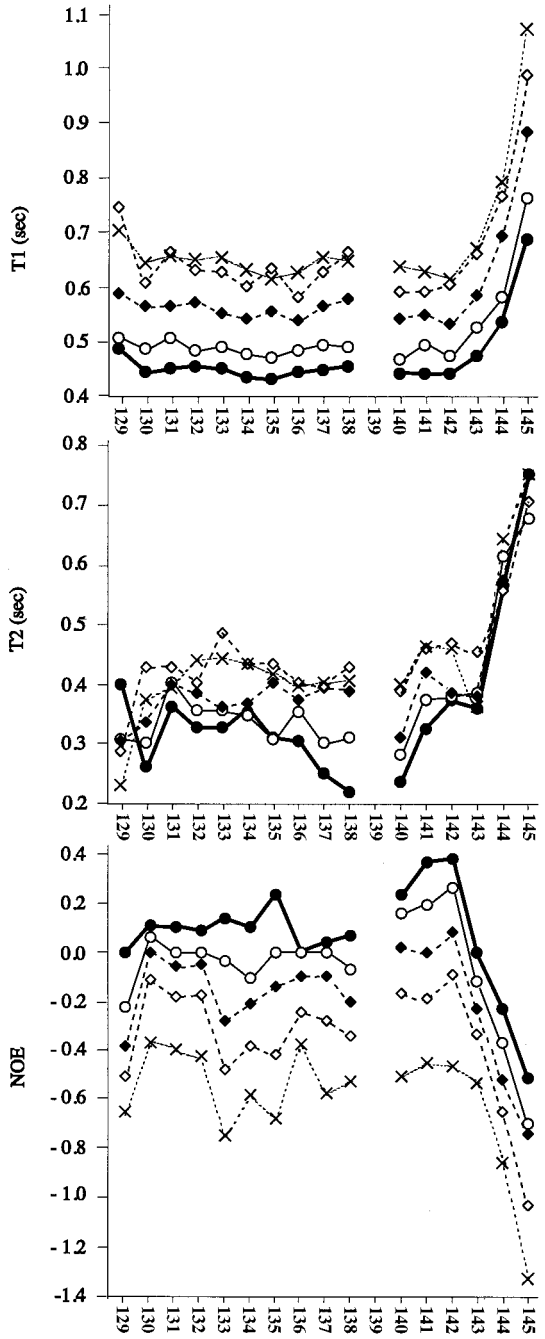

Figure 1. ^{15}N-relaxation parameters, T_1, T_2 and {^{1}H}-^{15}N NOE, versus amino acid residue for recombinant ^{15}N-labeled PAK 128–144(Hs145) measured at 500 MHz for various temperatures: 5 °C (thick line, filled circles), 10 °C (thin line, open circles), 15 °C (hatched line, filled diamonds), 20 °C (hatched line, open diamonds), and 25 °C (dotted line, crosses). Error bars (standard deviations calculated for each relaxation parameter) are not plotted to retain the visual clarity of the plots. However, standard deviations are listed with their associated T_1, T_2 and NOE values for each residue in Table S1 of the Supplementary material.

perature (see Figure 1). This behavior is likely a result of the contribution of slow time scale conformational exchange phenomena to measured T_2 transverse relaxation. Generally, T_2 should decrease monotonically with increasing molecular rotational correlation time, but rates of slow time scale (μs–ms) conformational exchange processes may either increase or decrease with temperature[1]. In the case where the rate of exchange (Rex) decreases with temperature, an increase in T_2 (in addition to that expected upon increased rotational tumbling) with temperature will be observed. In the case where Rex increases with temperature, T_2 may remain constant, or may even decrease with temperature if the increases in Rex exceed increases in T_2 caused by increased rates of rotational tumbling. Residues which display the shortest T_2 times at 5 °C (Thr[130], Phe[137], Ile[138] and Lys[140]) show the most pronounced increases in T_2 times with temperature, suggesting that Rex decreases with temperature. However, Cys[129], one residue removed from the N-terminus, shows a decrease in T_2 with temperature. This suggests that Rex increases substantially with temperature for this residue. The T_2 times for the C-terminal residues Lys[144] and Hs[145] show no significant changes with temperature, suggesting that increases in Rex with temperature can compensate an increase in T_2 due to more rapid molecular tumbling.

The temperature dependence of the $\{^1H\}$-^{15}N NOE provides a sensitive measure of the thermal stability of ordered regions within the PAK pilin peptide. The $\{^1H\}$-^{15}N NOE at 5 °C reaches maximum positive values for Lys[140], Gly[141] and Cys[142] of 0.23 ± 0.01, 0.37 ± 0.01, and 0.38 ± 0.01, respectively, suggesting that residues in the type II β-turn (Pro[139]-Lys-Gly-Cys[142]) are the most rigid in the peptide. A comparatively large NOE is also observed for Glu[135] (0.24 ± 0.01) within the type I β-turn (Asp[134]-Glu-Gln-Phe[137]), suggesting restricted mobility for the first turn as well. At temperatures greater than or equal to 10 °C, the NOE observed for Glu[135] is diminished to a value similar to the average value observed for other residues in the N-terminal half of the peptide (see Figure 1). This indicates that the first turn region is no more ordered than the N-terminal residues at temperatures greater than 5 °C. The second turn appears more temperature stable, as the ordering of this turn is maintained until 15 °C, above which the Lys[140], Gly[141] and Cys[142] NOEs diminish to intensities similar to those observed for other residues in the peptide (apart from the extreme C-terminal residues).

Field dependence of the ^{15}N-T_1 and T_2, and $\{^1H\}$-^{15}N NOE

The ^{15}N-T_1 and T_2 relaxation rates and the $\{^1H\}$-^{15}N NOE were measured at 5 °C for the recombinant PAK pilin peptide at 300, 500 and 600 MHz. These values are available as Supplementary material (Table S2) and are plotted in Figure 2. Theoretically, T_1^{300}, T_1^{500}, and T_1^{600} should be 385, 460, and 492 ms using the Lipari–Szabo one-time-scale spectral density function with $S^2 = 0.65$, $\tau_c = 2.2$ ns and $\tau_e = 130$ ps. The experimental averages of 423 ± 153, 445 ± 9, and 441 ± 16 ms for T_1^{300}, T_1^{500}, and T_1^{600}, respectively, compare well with these theoretical values. For T_2, the theoretical values are 319, 327, and 320 ms for T_2^{300}, T_2^{500}, and T_2^{600}, respectively, using $S^2 = 0.65$, $\tau_c = 2.2$ ns and $\tau_e = 130$ ps. The experimental averages of 299 ± 55, 337 ± 25, and 303 ± 30 ms, for T_2^{300}, T_2^{500}, and T_2^{600}, respectively, also compare well with these theoretical values. Finally, for $S^2 = 0.65$, $\tau_c = 2.2$ ns and $\tau_e = 130$ ps, the theoretical values of the $\{^1H\}$-^{15}N NOE are −0.42, +0.09, and +0.19 for NOE^{300}, NOE^{500}, and NOE^{600}, respectively. These agree within 95% confidence limits with the experimental averages of −0.24 ± 0.15, +0.17 ± 0.14, and +0.31 ± 0.22 for NOE^{300}, NOE^{500}, and NOE^{600}, respectively. However, all of the averages are slightly more positive than expected. This may be due to saturation transfer from water during the NOE experiment. The experimental averages for T_1, T_2, and $\{^1H\}$-^{15}N NOE exclude flexible residues (Cys[129], Ser[143], Lys[144] and Hs[145]) and residues with short T_2 values (Thr[130], Phe[137], Ile[138] and Lys[140]).

The bottom panel of Figure 2 shows that the pattern of NOEs roughly follows $NOE^{C-terminus} < NOE^{N-terminus} < NOE^{turns}$, independent of field. For example, the largest NOE^{500}s correspond to Glu[135], Lys[140], Gly[141] and Cys[142] in the turns, and the smallest NOE^{500}s correspond to Lys[144] and Hs[145] at the C-terminus. Similarily, the largest NOE^{300}s correspond to Glu[135] and Lys[140], and the smallest NOE^{300} values to Lys[144] and Hs[145]. The 600 MHz data shows a slightly different pattern; while the smallest NOE^{600}s are again measured for Lys[144] and Hs[145] at the C-terminus, the largest NOE^{600}s are measured for residues in the first (Asp[134], Glu[135], Phe[137]) and second (Lys[140], Gly[141] and Cys[142]) turns, as well as for Gln[133] just N-terminal to the first turn, and Ile[138]

[1]The temperature dependence of Rex is a function of the microscopic rate of exchange for the mechanism and the delay time between 180° pulses in the CPMG pulse train used to measure ^{15}N-T_2 (Mandel, 1996).

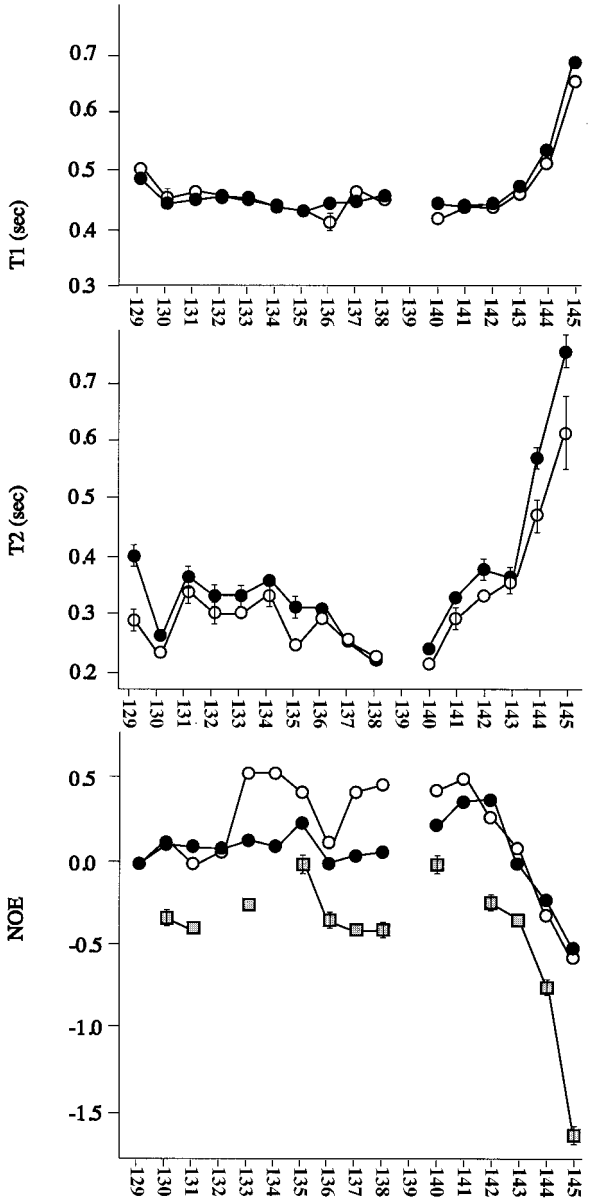

Figure 2. ^{15}N-relaxation parameters, T_1, T_2 and $\{^1H\}$-^{15}N NOE, versus amino acid residue for recombinant ^{15}N-labeled PAK 128–144(Hs145) measured at 5 °C for multiple fields: 300 MHz (grey squares), 500 MHz (black circles), and 600 MHz (open circles). Error bars (standard deviations calculated for each relaxation parameter) are plotted only when the bars are larger than the actual size of the symbol. The T_1^{300} and T_2^{300} values are not plotted due to large scatter in these data points. However, all T_1, T_2 and NOE values along with their associated standard deviations are listed for each residue in Table S2 of the Supplementary material.

in the hinge region between the two turns. The detection of these additional 'ordered residues' at 600 MHz versus 500 MHz (or 300 MHz) results from the superior signal-to-noise ratio of the 600 data, and the larger intrinsic value of the NOE at this field. Thus, ordered regions of the backbone are most clearly revealed in the 600 MHz data. With this in mind, the comparatively large NOE^{600}s detected for Gln^{133} and Ile^{138} suggest ordering of residues adjacent to (or sandwiched between) the two turns, and are consistent with the increased ordering of turn residues measured at all fields.

Model-free analysis

The 500 MHz and 600 MHz ^{15}N relaxation data acquired at 5 °C was analyzed using the model-free approach of Lipari and Szabo (1982a,b)[2]. τ_c^{500} and τ_c^{600} values at 5 °C were calculated from the average T_1^{500}/T_2^{500} and T_1^{600}/T_2^{600} ratios, respectively, using residues within one standard deviation of the mean (this included Cys^{129}, Ser^{131}, Asp^{132}, Gln^{133}, Asp^{134}, Glu^{135}, Gln^{136}, Gly^{141}, Cys^{142}, Ser^{143} and Lys^{144} for both sets of data). The calculated values of $\tau_c^{500} = 2.2 \pm 0.5$ ns and $\tau_c^{600} = 2.5 \pm 0.5$ ns were found to be in agreement with one another (within error) and comparable to τ_c values calculated for other peptides at low temperature. For example, $\tau_c = 2.5 \pm 0.1$ ns for the 20-residue peptide alamethicin in methanol at 5 °C (Spyracopoulos et al., 1996), and $\tau_c = 1.7 \pm 0.1$ ns for the 22-residue S-peptide in water at 10 °C (Alexandrescu et al., 1998).

Using the τ_c^{500} and τ_c^{600} values calculated above, the 500 MHz and 600 MHz relaxation data were first fit to a single-time-scale form of the spectral density function, and the model-free parameters S^2 and τ_e were calculated for all backbone amide N-H bond vectors in the PAK pilin peptide. The S^2 and τ_e values are available in Table S3 (500 MHz and 600 MHz data) and are plotted in Figure 3 (500 MHz data only). The average S^2 calculated at both fields was 0.6 ± 0.1, comparable to S^2 values calculated for the 22-residue S-peptide in water at 10 °C (Alexandrescu et al., 1998), but significantly lower than expected for a backbone amide within regions of well-defined

[2]Higher temperature relaxation data acquired at 500 MHz and 600 MHz could not be analyzed using the model-free approach, since the increased contribution of internal motions, τ_e, to the overall correlation time of the molecule made it impossible to extract a global optimum τ_c. Model-free analysis was also not possible for the 300 MHz data, even at 5 °C, as the poor signal-to-noise of the lower field instrument (no gradient accessories for sensitivity enhancement) resulted in non-convergence of the T_1/T_2 ratios.

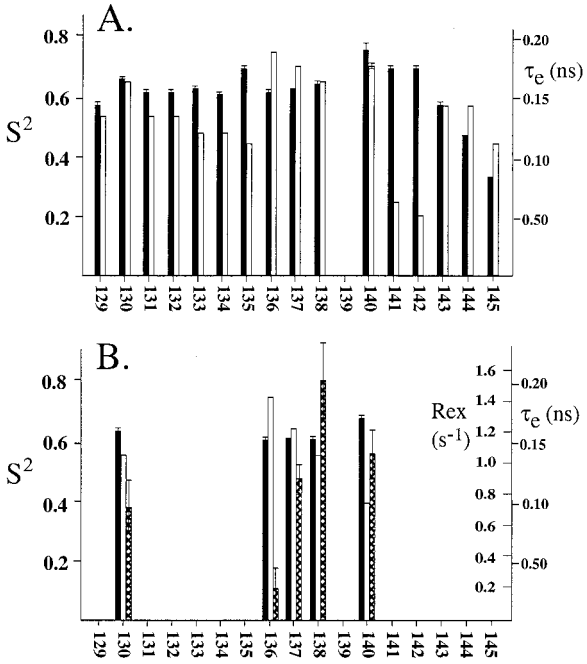

Figure 3. Model-free order parameters as a function of residue number for recombinant ^{15}N-labeled PAK 128–144(Hs145) measured at 500 MHz and 5 °C. (A) Order parameters (S^2, black bars) and internal correlation times (τ_e, white bars) calculated using the single-time-scale form of the spectral density function; (B) order parameters (S^2, black bars), internal correlation times (τ_e, white bars), and exchange rates (Rex, cross-hatched bars) calculated using the single-time-scale form of the spectral density function and including exchange effects. Standard deviations calculated for each parameter are plotted as error bars. Values of S^2, τ_e and Rex along with their associated standard deviations are listed for each residue in Table S3 of the Supplementary material.

secondary structure in a protein at 5 °C ($S^2 \sim 0.9$). Individual S^2 values vary across the peptide sequence, indicating regions of differing backbone flexibility. For example, the low S^2 values for residues Lys^{144} and Hs^{145} ($S^2 = 0.47$ and 0.34, respectively, at 500 MHz, and $S^2 = 0.46$ and 0.35, respectively, at 600 MHz) suggest that motions at the C-terminus are less restricted than motions within the disulfide loop region. Within the disulfide loop, the most ordered residues are Glu^{135} ($S^2 = 0.68$ at 500 MHz, and $S^2 = 0.71$ at 600 MHz) and Phe^{137} ($S^2 = 0.72$ at 600 MHz) located within the first β-turn (Asp^{134}-Glu-Gln-Phe^{137}); Lys^{140}, Gly^{141} and Cys^{142} ($S^2 = 0.75$, 0.68 and 0.68, respectively, at 500 MHz, and $S^2 = 0.66$, 0.75 and 0.68, respectively, at 600 MHz) located within the second β-turn (Pro^{139}-Lys-Gly-Cys^{142}); and Ile^{138} ($S^2 = 0.75$ at 600 MHz) situated between the two turns. These results imply that the regions encompassing the two turns, and in particular the second turn, are the most ordered regions of the PAK pilin peptide.

In order to determine if the relaxation data could be better fit by including the effects of conformational exchange, the parameter Rex was included in the calculation of S^2 and τ_e using the one-time-scale spectral density function (Clore et al., 1990). These S^2, τ_e and Rex values are available in Table S3 and are plotted in Figure 3 for only those residues where the same or better fits were obtained on the basis of a χ^2 calculation[3,4]. Exchange terms were required to better fit relaxation data for residues Thr^{130}, Gln^{136}, Phe^{137}, Ile^{138} and Lys^{140} at 500 MHz (Rex^{500} = 0.7, 0.2, 0.9, 1.5 and 1.1 Hz, respectively), and Cys^{129}, Thr^{130}, Glu^{135}, Phe^{137}, Ile^{138} and Lys^{140} at 600 MHz (Rex^{600} = 0.5, 0.9, 0.4, 0.5, 0.8 and 1.2 Hz, respectively). Thus, the 500 and 600 MHz data yielded Rex terms for the same two regions of the peptide sequence (residues 129–130 and residues 135–140), with the largest Rex terms at both fields being associated with residues Thr^{130}, Ile^{138} and Lys^{140}. Unfortunately, the lack of a strong field dependence for these Rex terms precluded a more accurate evaluation of either Rex^{500} or Rex^{600} using the method outlined by Farrow and co-workers (1995).

[3]Relaxation parameters calculated from the spectral density functions were compared to experimental values using a χ^2 function defined as (Farrow et al., 1994):

$$\chi^2 = (T_{1c} - T_{1e})^2/\sigma_{T1}^2 + (T_{2c} - T_{2e})^2/\sigma_{T2}^2 + (NOE_c - NOE_e)^2/\sigma_{NOE}^2$$

where the subscripts c and e represent calculated and experimentally determined relaxation parameters, respectively, and σ_{T1}, σ_{T2} and σ_{NOE} are estimates of the standard deviation of the experimentally determined parameters. Nonlinear least-squares optimizations were performed for the variables in the single-time-scale form of the spectral density function: with S^2 and τ_e used as fitting parameters (two-parameter fit); and with S^2, τ_e and Rex used as fitting parameters (three-parameter fit). The appropriate form of the spectral density function was decided on a per residue basis using the following criteria: all three relaxation parameters must be fit with 95% confidence limits, each of the fitting parameters must exceed their calculated error, if more than one of the spectral density functions satisfied both conditions, then the model with the lowest χ^2 would be chosen.

[4]Where the inclusion of an additional Rex parameter was required to better fit the relaxation data for a particular residue, an F-statistic was calculated. The F-statistic assesses whether an improvement in fit is significant or arises merely due to the incorporation of an additional parameter (Rex) in the fit. For all residues where the inclusion of Rex led to an improvement in the fit to the relaxation data, the improvement was found to be statistically significant.

Temperature dependence of the spectral density function

Model-free analysis often provides a means of assessing the contributions of internal motions and conformational exchange to the spin relaxation of globular proteins in solution. However, there are limitations that arise from inherent assumptions. The overall molecular reorientation must be isotropic and independent from fast internal motions, whose contributions to relaxation are negligible ($\tau_c \gg \tau_e$). These assumptions do not necessarily hold for small flexible peptides in solution, especially at temperatures greater than 5 °C, above which the concept of a global τ_c is suspect due to a lack of regular secondary structure. An alternative relaxation analysis approach for characterizing molecular dynamics at multiple temperatures is provided by spectral density mapping, which has the advantage that it makes no assumptions about the separability of the time scales between the motions, and allows the possibility of sizeable contributions to relaxation from high-frequency motions.

In general, J(0) is proportional to the local correlation time of the backbone nitrogen[5] (Peng and Wagner, 1992a). Thus, it is possible to interpret temperature effects on the basis of changes in local correlation times. However, this interpretation is valid only in the absence of conformational exchange phenomena, which can lead to shortenening of T_2 times, and therefore larger values of J(0). In certain cases, conformational exchange phenomena can contribute significantly more to the value of J(0) than the local correlation time (Davis and Agard, 1998). The contribution of slow motions (μs–ms) to T_2 must therefore be carefully scrutinized.

The spectral density values, J(0), $J(\omega_N)$ and $J(\omega_H)$, were calculated from the 500 MHz relaxation parameters measured for the recombinant PAK pilin peptide at 5, 10, 15, 20, and 25 °C. These values are available in Table S4 and are plotted in Figure 4. Most residues (with the exception of Cys^{129}, Lys^{144} and Hs^{145}) show a general decrease in both J(0) and $J(\omega_N)$ with increasing temperature, accompanied by a small but discernible increase in $J(\omega_H)$. Thus, higher frequency motions are making a greater contribution to the spectral density function at higher temperatures, leading to an overall 'flattening' of the spectral density curve.

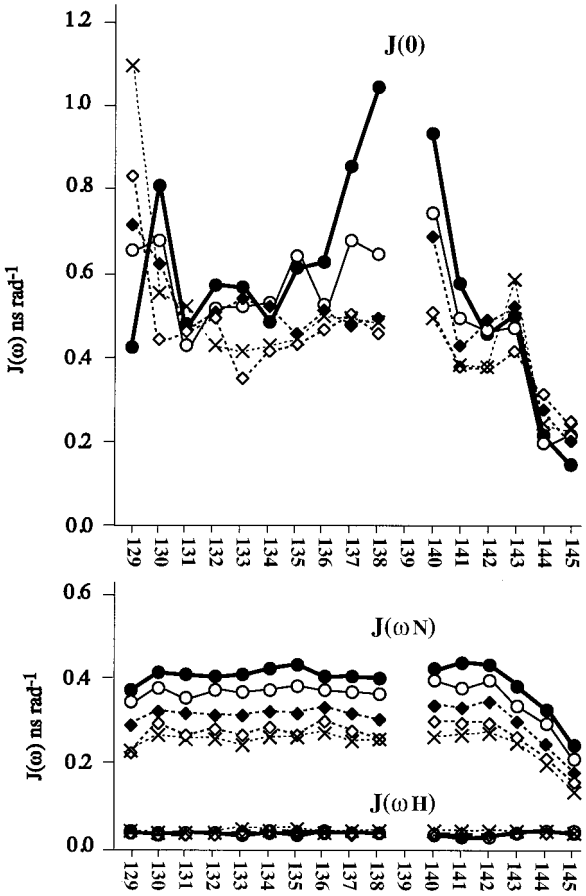

Figure 4. J(ω) spectral density values, J(0), $J(\omega_N)$ and $J(\omega_H)$, versus amino acid residue for recombinant ^{15}N-labeled PAK 128–144(Hs145), calculated from the ^{15}N-relaxation parameters measured at 500 MHz for various temperatures: 5 °C (thick line, filled circles), 10 °C (thin line, open circles), 15 °C (hatched line, filled diamonds), 20 °C (hatched line, open diamonds), and 25 °C (dotted line, crosses). Error bars (standard deviations calculated for each spectral density value) are not plotted for visual clarity. However, standard deviations are listed with their associated J(0), $J(\omega_N)$ and $J(\omega_H)$ values for each residue in Table S4 of the Supplementary material.

Residues Thr^{130}, Phe^{137}, Ile^{138} and Lys^{140} show the largest J(0) values at 5 °C, consistent with their low T_2 values of 262 ± 10, 252 ± 5, 220 ± 11 and 238 ± 7 ms, respectively, compared to the average value of 360 ms. The J(0) values for these residues markedly decrease with increasing temperature, such that they merge with the average J(0) value for all residues at

[5] J(0) is the limiting value of J(ω) for time scales in which G(τ) has decayed to zero, i.e. G(0). All amide NH vectors have the boundary values of G(0) = 1/5 and G(∞) = 0, independent of the specific dynamics. Thus, J(0) is proportional to τ_c as defined by:

$$J(0) = 2\int_0^\infty G(\tau)d\tau = 2G(0)\tau_c = 2/5\tau_c$$

Since J(ω) values reflect both the global and internal motions of the molecule, there are no a priori assumptions about the separability of time scales.

temperatures greater than 15 °C (Figure 4). For example, at 5 °C, residues Thr^{130}, Phe^{137}, Ile^{138} and Lys^{140} show J(0) values of 0.81 ± 0.04, 0.86 ± 0.03, 1.05 ± 0.07, and 0.94 ± 0.04 ns rad^{-1}, significantly larger than the average J(0) of 0.58 ns rad^{-1}. In contrast, at 25 °C, residues Thr^{130}, Phe^{137}, Ile^{138} and Lys^{140} show J(0) values of 0.56 ± 0.01, 0.50 ± 0.01, 0.49 ± 0.02, and 0.50 ± 0.01 ns rad^{-1}, similar to the average J(0) of 0.48 ns rad^{-1}. While the temperature dependence of J(0) for residues Thr^{130}, Phe^{137}, Ile^{138} and Lys^{140} is due in part to decreases in local correlation times (presumably as the peptide backbone unfolds), it is probably dominated by decreases in Rex with temperature. Support for the importance of changes in the rates of μs–ms time scale phenomena in determining the temperature behavior of J(0) is evidenced by the large increases in T_2 with temperature (Figure 1). For example, at 5 °C the average T_2 for residues in the disulfide loop (129–142) is 310 ms, which is larger than the average T_2 of 245 ms for residues Thr^{130}, Phe^{137}, Ile^{138} and Lys^{140}. By comparison, the average T_2 for Thr^{130}, Phe^{137}, Ile^{138} and Lys^{140} is 396 ms at 25 °C, which is much closer to the average T_2 of 415 ms for residues in the disulfide loop (129–142). In addition, an Rex term was required in the model-free analysis to fit the relaxation data for these residues at 5 °C.

In contrast to the J(0) temperature behaviour exhibited by Thr^{130}, Phe^{137}, Ile^{138} and Lys^{140}, the J(0) value of Cys^{129} is observed to markedly increase with temperature. An increase of J(0) with temperature can be caused by an increase in local correlation time. However, this is unlikely as it would imply that the peptide backbone becomes less flexible with increasing temperature. Thus, increases in J(0) with temperature are likely to be dominated by increases in Rex. Large increases in Rex with temperature are consistent with the observed decrease in Cys^{129} T_2 with temperature noted earlier (Figure 1). The J(0) values of Lys^{144} and Hs^{145} also show small but significant increases with temperature, which may be caused by smaller increases in Rex with temperature that are still sufficiently large to override decreases in the local correlation time for these C-terminal residues. This is consistent with the relative insensitivity of the Lys^{144} and Hs^{145} T_2 times to temperature (Figure 1).

The fact that no Rex terms were required to better fit the relaxation data of Cys^{129}, Lys^{144} and Hs^{145} at 5 °C does not mean that exchange processes do not exist for these residues, only that they do not exist within the μs–ms time scale window at this temperature. The 'emergence' of increasing Rex contributions at higher temperatures might then be explained by increases in microscopic exchange rates of these processes, accompanied by a shifting of time scales into the observable window (seconds to milliseconds, for example). Increasing contributions of Rex to T_2 exchange broadening would result in the increases in J(0) with temperature observed for these residues.

Spectral density mapping at multiple fields

The measurement of the ^{15}N relaxation parameters at multiple fields allows sampling of the spectral density function at multiple frequencies, and therefore provides a more detailed picture of the distribution of motions associated with the dynamics of a backbone amide N-H bond vector than would be provided from relaxation measurements at just one field. Measurement of ^{15}N-T_1 and T_2 relaxation rates and {^{1}H}-^{15}N NOE at 300, 500 and 600 MHz allows a sampling of the spectral density function at seven different frequencies, roughly 0, 30, 50, 60, 300, 500 and 600 MHz, corresponding to the J(0), J(ω_N) and J(ω_H) values associated with the three fields. J(0), J(ω_N) and J(ω_H) values as a function of field are given in Table S5 and are plotted in Figure 5. The pattern for each residue roughly follows $J(0)^{300} \approx J(0)^{500} \approx J(0)^{600} > J(30) > J(50) > J(60) > J(300) > J(500) > J(600)$, as predicted by theory.

There is general agreement between the 500 and 600 MHz data in that maximal J(0) values are observed for the same residues (Thr^{130}, Phe^{137}, Ile^{138} and Lys^{140}), consistent with their lower than average T_2 values. The average J(0) for the 600 MHz data is 0.7 ± 0.2 ns rad^{-1}, and 0.6 ± 0.2 ns rad^{-1} for the 500 MHz data. Generally, J(0) is expected to be field independent for isotropic rotational tumbling of a molecule. However, if conformational exchange contributes to T_2, J(0) will exhibit a field dependence (Farrow et al., 1995). For example, $J(0)^{600} = 0.69$ ns rad^{-1} versus $J(0)^{500} = 0.43$ ns rad^{-1} is observed for Cys^{129}, and $J(0)^{600} = 0.83$ ns rad^{-1} versus $J(0)^{500} = 0.61$ ns rad^{-1} is observed for Glu^{135}.

Figure 6 shows the J(ω) spectral density values sampled at 0, 30, 50, 60, 300, 500 and 600 MHz for selected residues in the recombinant PAK pilin peptide. The spectral density curves for each residue appear 'flattened', that is, the values of the high frequency J(ω_H) and J($\omega_H \pm \omega_N$) terms are comparable to the spectral density at lower frequencies (J(0) and J(ω_N)). This suggests considerable internal mobility of backbone nitrogens, consistent with the dynamics

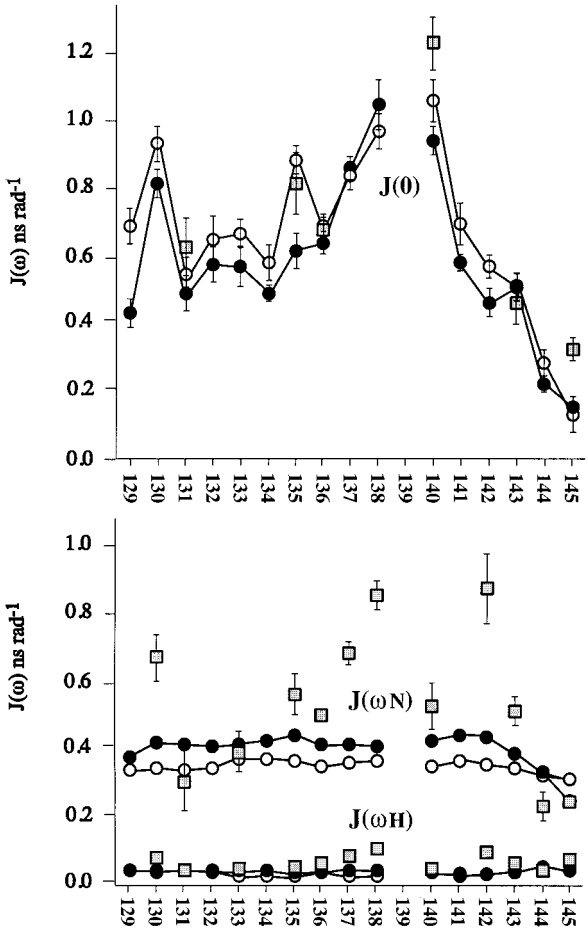

Figure 5. J(ω) spectral density values, J(0), J(ω_N) and J(ω_H), versus amino acid residue for recombinant ^{15}N-labeled PAK 128–144(Hs145), calculated from the ^{15}N-relaxation parameters measured at 5 °C for multiple fields: 300 MHz (grey squares), 500 MHz (filled circles), and 600 MHz (open circles). Error bars (standard deviations calculated for each spectral density value) are plotted only when the bars are larger than the actual size of the symbol. J(0), J(ω_N) and J(ω_H) values along with their associated standard deviations are listed for each residue in Table S5 of the Supplementary material.

of a flexible peptide in solution. However, variations in the values of J(0) also indicate differences in the dynamic behaviour of individual residues. These differences are best reflected in the J(50)/J(0)av[6] ratios, which are 0.55 for Thr^{130} and 0.74 for Ser^{131} in the region N-terminal to the β-turns, 0.61 for Gln^{136} and 0.30 for Phe^{137} in the first β-turn, 0.46 for Ile^{138} in the 'hinge region' between turns, 0.39 for Lys^{140} and 0.84 for Cys^{142} in the second β-turn, and 0.73 for Lys^{144} in the flexible C-terminus. Thus, the largest J(50)/J(0)av ratios are measured for relatively unordered regions of the peptide (Ser^{131} and Lys^{144}), whereas the smallest J(50)/J(0)av ratios are measured for regions of the peptide where both order (β-turn conformation) and exchange coincide (Phe^{137} and Lys^{140}). Notice that relatively unordered regions of the peptide undergoing exchange (Thr^{130}) display even smaller J(50)/J(0)av ratios than ordered regions of the peptide not undergoing exchange (Cys^{142}). This underlines the importance of interpreting spectral density curves on the basis of contributions from both fast internal motions (ps–ns) and slow exchange (μs–ms) behaviour.

[6]J(0)av is defined as J(0)av = [J(0)^{300} + J(0)^{500} + J(0)^{600}]/3, where the superscript indicates the field. Using a J(0) averaged over all three fields improves the accuracy of the J(50)/J(0)av ratios.

Discussion

Mechanisms of conformational exchange

The ^{15}N relaxation measurements for the PAK pilin peptide at 5 °C and 500 MHz offer evidence of conformational exchange on the μs–ms time scale; manifested as shorter than average ^{15}N-T_2 times for Thr^{130}, Gln^{136}, Phe^{137}, Ile^{138} and Lys^{140}, and detected as Rex exchange terms required to better fit these residues in the model-free analysis. The existence of short T_2 times and Rex terms for two separated regions of the peptide backbone (residues 130 and 136–140) indicates at least two separate conformational exchange mechanisms, for which possible mechanisms will now be discussed.

The Rex term calculated for Thr^{130} may result from isomerization of the neighbouring Cys^{129}-Cys^{142} disulfide bond. Disulfide bond isomerization with μs–ms time scale dynamics has been observed in several peptides and proteins. Time scales for these motions have varied, being 20–200 μs at 35 °C for Cys^{17}-Cys^{40} in toxin α from *Naja nigricollis* (Zinn-Justin et al., 1997), 1–2 ms at 36 °C for Cys^{14}-Cys^{38} in BPTI (Szyperski et al., 1993), and 10–30 μs over a wide range of temperatures (0–55 °C) for a disulfide bridged cyclic octapeptide (Kopple et al., 1988). Rex exchange terms were included in the ^{15}N relaxation data of the C-terminal domain of the human α3-chain from type VI collagen to account for μs–ms time scale motions of 11 residues in the vicinity of the Cys^{20}-Cys^{44} disulfide bond (Sørensen et al., 1997). Interestingly, another study found that reducing the disulfide in a BPTI mutant (Y35G) significantly decreased the number of backbone amides displaying large T_2 relaxation rates (Beeser et al., 1998).

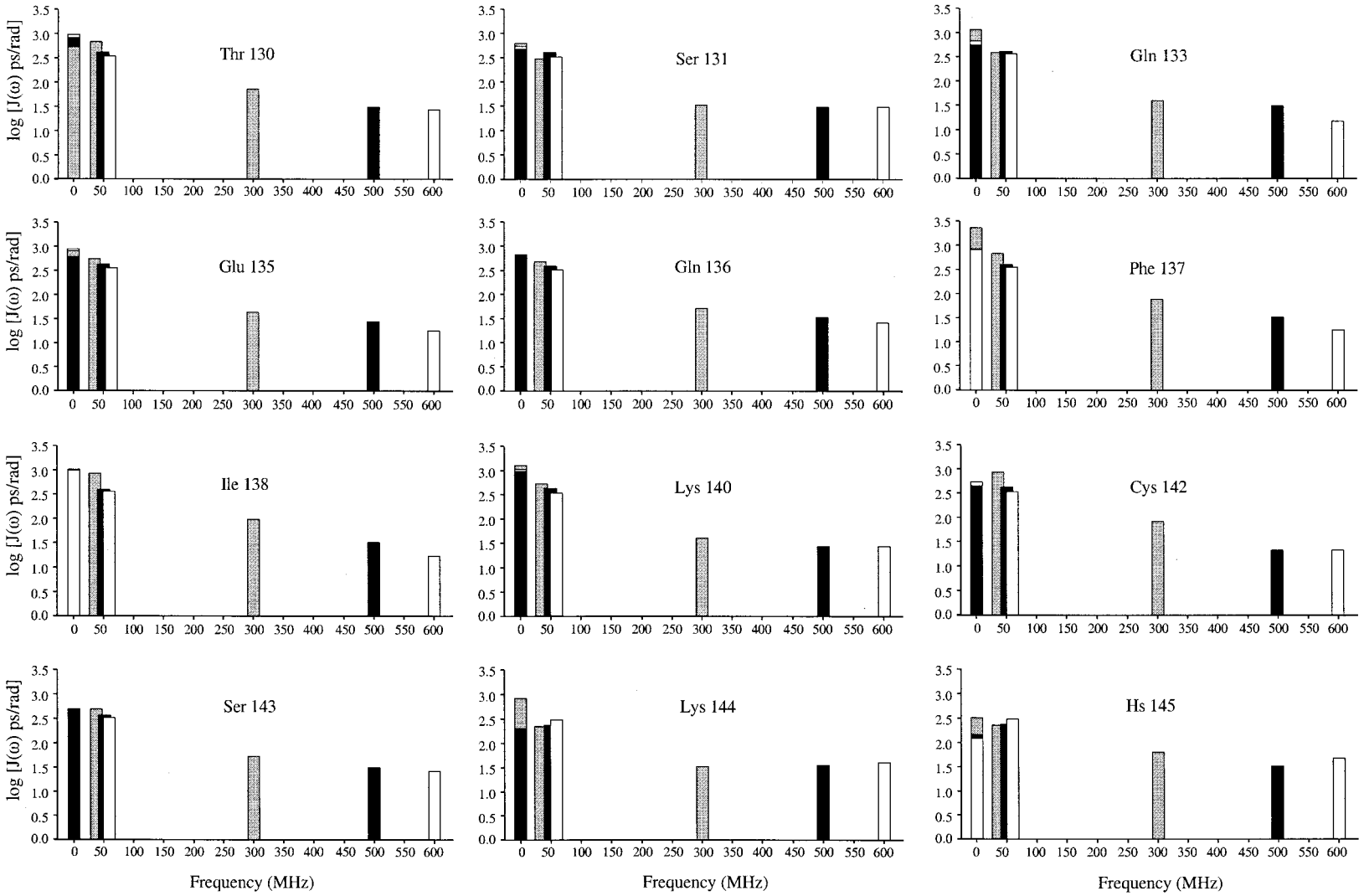

Figure 6. Log [J(ω)] spectral density values versus frequency for selected residues of recombinant ^{15}N-labeled PAK 128–144(Hs145). Log [J(ω)] is sampled at seven frequencies; 0, 30, 50, 60, 300, 500 and 600 MHz, corresponding to the J(0), J(ω_N) and J(ω_H) values calculated from the ^{15}N-relaxation parameters measured at 5 °C for multiple fields: 300 MHz (shaded bars), 500 MHz (black bars), and 600 MHz (white bars).

Disulfide bond isomerization has been directly observed in BPTI as a doubling of resonances in the ^{15}N-edited HSQC spectrum of this protein (Otting et al., 1993). According to a model representation of the two different disulfide bond arrangements in the major and minor conformations of BPTI, isomerization occurs as a result of a $-120°$ rotation around the Cα–Cβ bond of one of the cysteines. While this places the Hβ protons of one of the cysteines into two possible arrangements, it leaves the Hβ protons of the other cysteine in the same position in both isomers. According to this model, the Hα and Hβ resonances of the cysteine undergoing Cα–Cβ rotation should be doubled, whereas the Hα and Hβ resonances of the other cysteine should remain as single resonances. This appears to be the situation with the *trans* isomer of the PAK pilin peptide at pH 4.5, where the resonances of only one cysteine, Cys^{129}, are observed to be split. A close examination of the ^{15}N-edited NOESY HSQC spectrum of the recombinant PAK pilin peptide (Campbell et al., 2000) shows a doubling of the ^{15}N, NH, Hα (F2, F1, F3) cross peak for Cys^{129} for the *trans* isomer. This suggests that the Cα–Cβ bond of Cys^{129} is undergoing conformational exchange, placing the Hα into two chemically different environments.

The Rex terms associated with Gln^{136}, Phe^{137}, Ile^{138} and Lys^{140} likewise indicate that the backbone region spanned by Gln^{136}-Phe^{137}-Ile^{138}-Pro^{139}-Lys^{140} is undergoing motions on the μs–ms time scale, with exchange contributions 'peaking' around Ile^{138}. While *cis/trans* isomerization around the central Ile^{138}-Pro^{139} peptide bond (Campbell et al., 1995) would certainly affect this region of the backbone, X-Pro isomerization cannot account for the presence of the Rex terms as it occurs on a time scale too slow to contribute to exchange broadening. Even for extended linear oligopeptides, exchange rates have been measured to be as slow as 10^{-2} to 10^{-3} s^{-1} at 25 °C (Grathwohl and Wüthrich, 1981). The detection of separate *cis* and *trans* resonances for both the synthetic (Campbell et al., 1995, 1997b) and recombinant (Campbell et al., 1997a) PAK pilin peptides over a range of temperatures confirms a time scale of seconds to minutes for this process.

Other exchange mechanisms which might affect residues 136–140 and which occur on a much faster time scale include: 180° phenyl ring flips about the Cβ-Cγ bond of Phe^{137}; bending motions around the hinge residue, Ile^{138}, which affects the relative orientation of the two turns; or conformational exchange within the turns themselves. 'Hinge-bending motions' between subdomains of human α-TGF have been invoked to explain ^{15}N-T_2 exchange broadening (Li et al., 1995). Conformational exchange in ordered turns has been proposed to cause T_2 exchange broadening in both ^{15}N relaxation measurements (Nicholson et al., 1995; Barbar et al., 1998; Kontaxis et al., 1998; Crump et al., 1999; LiWang et al., 1999) and ^{13}C Cα relaxation measurements (Beglova et al., 1998).

While conformational exchange may be occurring within the β-turns of the PAK pilin peptide, this seems unlikely as the configurations of these turns (a type I β-turn spanning Asp^{134}-Glu-Gln-Phe^{137} and a type II β-turn spanning Pro^{139}-Lys-Gly-Cys^{142}) are well defined by the relative strengths of the $d_{\alpha N}(2,3)$, $d_{NN}(2,3)$ and $d_{\beta N}(2,4)$ cross peaks (Campbell et al., 1995, 1997a). This is in agreement with the NMR solution structure of the *trans* isomer of the synthetic PAK 128–144 peptide which shows a type I and a type II β-turn spanning these same residues (Campbell et al., 1995). In addition, the NMR solution structures of the *trans* isomers of two other synthetic peptides, PAO 128–144 and KB7 128–144, derived from the corresponding C-terminal receptor binding regions of strains PAO and KB7 *P. aeruginosa* pilin showed the same two sequential β-turns, conserved in both sequence and configuration despite limited sequence homology (Campbell et al., 1995).

Bending motions around the hinge residue, Ile^{138}, offer a more plausible exchange mechanism for residues 136–140. Evidence for this mechanism comes again from a comparison of the NMR solution structures of the *trans* isomers of the PAK, PAO and KB7 synthetic peptides. These structures show significant variation in the relative orientations of the first type I β-turn to the second type II β-turn (Campbell et al., 1995), demonstrating the potential of large-scale hinge motions around residue 138 in each sequence. Since each of these peptides binds to a cross-reactive monoclonal antibody Mab PAK-13 with similar affinity (μmolar; Sheth et al., 1995), it has been suggested that hinge rotations about Ile^{138} might place the two turns into the same relative alignment for binding (Campbell et al., 1995). However, ^{1}H NMR-monitored titrations of these pilin peptides with Mab PAK-13 (Campbell et al., 1997b) showed no significant changes in the arrangements of their hydrophobic pockets or turns free in solution versus bound to antibody.

Motions about the Cβ-Cγ bond of Phe^{137} offer a third plausible exchange mechanism. Ring flipping

about the Cβ-Cγ bond of aromatic residues has been measured on the μs–ms time scale (Wagner et al., 1987; Nall and Zuniga, 1990). Such slow motions around the Cβ-Cγ bond of Phe[137] could theoretically lead to exchange broadening of surrounding residues, if this motion were coupled to other motions in the peptide (the 180° ring flip alone is not expected to cause exchange broadening of surrounding residues, as the two conformational end-states of the ring flip are identical). The NMR solution structure of the *trans* isomer of the PAK pilin peptide shows a well-packed hydrophobic core comprising the side chains of Phe[137], Ile[138] and Pro[139] (Campbell et al., 1995). A full 180° ring flip about the Cβ-Cγ bond of Phe[137] might therefore need to be coupled to a 'breathing motion' of the hydrophobic pocket, so as to loosen local structure. A coupling of Phe[137] ring motions and hydrophobic pocket motions on the μs–ms time scale could account for the exchange broadening observed for Ile[138] and Pro[139] (and to a lesser extent, Gln[136] and Lys[140]).

Solvent exchange

Exchange of backbone amide hydrogens with bulk water occurs for several residues in the peptide, specifically Cys[129], Lys[144] and Hs[145] at the N- and C-termini of the peptide. However, this is not detected as Rex contributions to the ^{15}N-T_2 rates measured at low pH and temperature (pH 5, 5 °C), as it occurs at time scales too slow to contribute to exchange broadening (seconds–hours; Bai et al., 1993). Hydrogen exchange rates can be increased (and time scales decreased) by increasing either the pH or the temperature of the sample (Englander et al., 1979). Bai and co-workers (1993) measured increases in k_{HX} of up to a factor of 10^2 for several of their peptides (at 5 °C), as the pH was increased from 5.0 to 7.0. When this 10^2 increase in k_{HX} is combined with a factor of at least 10^1 as temperature is increased from 5 °C to 40 °C[7], time scales may be diminished by a factor of 10^3. For small peptides or unstructured regions of proteins, this may be sufficient to shift time scales into the millisecond upper limit for detection. At temperatures of 35 °C (at pH 7), exchange rates have been measured to be greater than $> 20\ s^{-1}$ for the disordered central helix of calmodulin (Ikura et al., 1991) and calcineurin (Grzesiek and Bax, 1993a). This corresponds to a time scale of 10–100 ms, just within the time scale window detectable by ^{15}N-T_2 measurements.

An increase in the k_{HX} rates of Cys[129], Lys[144] and Hs[145] from seconds to milliseconds time scales may be a source of the decreases in the ^{15}N-T_2 times (Figure 1) and increases in the J(0) values (Figure 4) measured for these residues as temperature is increased from 5 °C to 25 °C. However, to the best of our knowledge there are no documented cases of millisecond time scale solvent exchange processes leading to exchange broadening of the attached amide ^{15}N resonance. Thus, it is not clear at this time if the temperature-induced decreases in ^{15}N-T_2 are mediated by exchange broadening, or by other mechanisms similar to the effects of solvent exchange on the measurement of ^{15}N-T_1 and {^{1}H}-^{15}N NOE (Grzesiek and Bax, 1993b; Skelton et al., 1993; Zidek et al., 1999)[8].

If increased rates of solvent exchange were responsible for the decreases in the ^{15}N-T_2 times observed for Cys[129], Lys[144] and Hs[145], then the ^{15}N-T_2 times of these residues should also decrease with increasing pH (at constant temperature). In order to test this hypothesis, 500 MHz ^{15}N-T_2 relaxation times were measured at pH 7.2, and the values were compared to the ^{15}N-T_2 relaxation times previously measured at pH 4.5. Figure 7 shows the 500 MHz ^{15}N-T_1 and T_2 times and the {^{1}H}-^{15}N NOE plotted at pH 4.5 and pH 7.2. The N-terminal amide proton resonances of both Lys[128] and Cys[129] are completely exchanged at the higher pH. For all remaining residues (130–145), ^{15}N-T_1 relaxation times are similar within error, whereas ^{15}N-T_2 relaxation times are on average 100 ms shorter at pH 7.2 (260 ms) than at pH 4.5 (360 ms). A comparison of the individual T_2 values across the sequence shows that ^{15}N-T_2 times are most decreased for residues near the N- and C-terminus. This pH-sensitive pattern is consistent with a base-catalyzed solvent exchange mechanism.

Interestingly, the turn residue Glu[135] also displays a significantly decreased T_2 at higher pH (310 ms at pH 4.5 versus 200 ms at pH 7.5). Whether this change in dynamics is due to the ionization state of

[7]According to the Arrhenius relationship, the activational energy of Ea = 17.5 kcal/mol measured for base catalysis (Englander and Kallenbach, 1984) produces a 10-fold rate increase as temperature is increased from 5 °C to 40 °C.

[8]Solvent exchange can lead to an NOE enhancement if delays between scans are too short, preventing full recovery of amide proton and amide nitrogen z magnetization (Grzesiek and Bax, 1993b; Skelton et al., 1993). Solvent exchange can theoretically also lead to shortened ^{15}N-T_1s if the exchange is fast enough to occur between the 180° pulses applied during the relaxation delay (Zidek et al., 1999). If these pulses are spaced 5 ms apart, exchange rates would have to approach $\sim 200\ s^{-1}$ to lead to shortening of ^{15}N-T_1s.

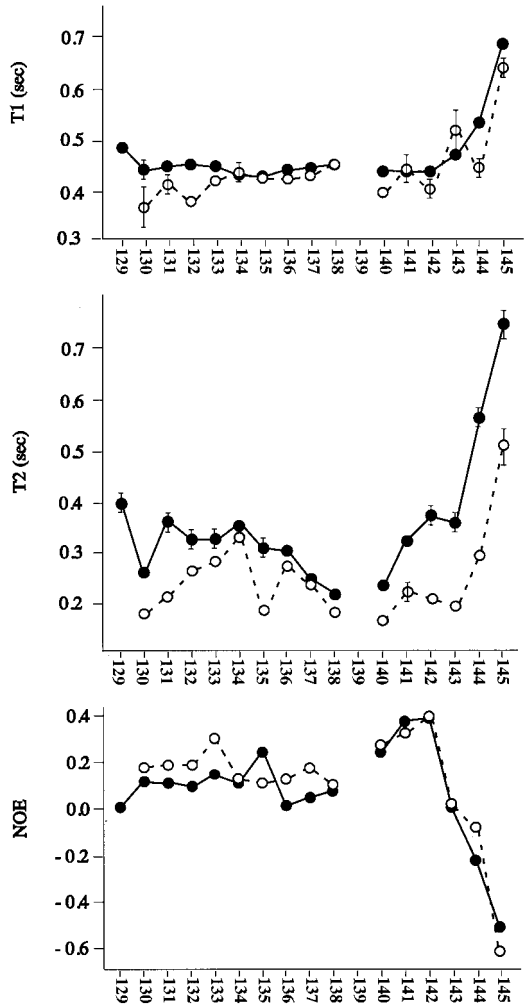

Figure 7. ^{15}N-relaxation parameters, T_1, T_2 and $\{^1H\}$-^{15}N NOE, versus amino acid residue for recombinant ^{15}N-labeled PAK 128–144(Hs145) measured at 5 °C for pH 4.5 (filled circles) versus pH 7.4 (hatched line, open circles). Error bars (standard deviations calculated for each relaxation parameter) are plotted only when the bars are larger than the actual size of the symbol. pH 7.4 T_1, T_2 and NOE values along with their associated standard deviations are listed for each residue in Table S6 of the Supplementary material.

the glutamyl side chain (pKa $\approx$ 4.5)[9] or an artifact due to increased base-catalyzed solvent exchange is unknown at this time. However, a comparison of the $\{^1H\}$-^{15}N NOE plotted at pH 4.5 and pH 7.2 does reveal a slightly different pattern of NOEs for residues 133–137 surrounding the first turn, whereas the NOE values for the second turn are virtually identical at pH 4.5 and 7.2. In particular, the NOE for Glu^{135} is significantly larger at pH 4.5 (0.24) than it is at pH 7.5 (0.12). This may be a reflection of a more stable turn conformation spanning residues Asp^{134}-Glu-Gln-Phe^{137} [10] at pH 4.5. However, rapid exchange of backbone amide protons with solvent protons leads to increased $\{^1H\}$-^{15}N NOE values (Grzesiek and Bax, 1993b; Skelton et al., 1993), and this may explain the different $\{^1H\}$-^{15}N NOE values at pH 4.5 compared to pH 7.2.

Role of backbone motions in PAK pilin peptide immunogenicity

There is evidence that the type I and type II β-turns spanning residues Asp^{134}-Glu-Gln-Phe^{137} and Pro^{139}-Lys-Gly-Cys^{142}, respectively, occur in the epitope region of the PAK pilus and constitute the structural element for strain-specific or cross-reactive antibody recognition (Sheth et al., 1995; Campbell et al., 1997b). There is also evidence that these β-turns are involved in the recognition of a glycosphingolipid cell surface receptor common to many strains of *P. aeruginosa* (Wong et al., 1995; Campbell et al., 1997b). The $\{^1H\}$-^{15}N NOEs measured at 5 °C for the recombinant PAK pilin peptide at multiple fields show the β-turns to be the most ordered and structured regions of the peptide. If the turns were very rigid in solution ($S^2 > 0.8$), there would be no entropic cost upon antibody (or receptor) binding. However, this would amount to a 'lock-and-key' model for peptide–antibody interaction, where the dynamics of the system is essentially ignored. In contrast, the 'induced fit' model allows for changes in the structure and dynamics of either the peptide or antibody, allowing for a 'fine-tuning' of the binding affinity.

Motions likely to have significance in an induced fit are those within the μs–ms time scale, or slow motions involving conformational exchange. Active sites or binding pockets of proteins experience conformational exchange processes, which are either stabilized (Nicholson et al., 1992; Akke et al., 1993; Davis et al., 1997; Davis and Agard, 1998) or increased (Farrow et al., 1994; Epstein et al., 1995; Stivers et al., 1996; Hyre and Klevit, 1998) by ligand binding, thereby increasing or decreasing the loss of entropy upon bind-

[9] A ^{1}H NMR-monitored pH titration of the synthetic version of the PAK pilin peptide showed titration of the backbone amide resonance of Glu^{135} from 8.25 ppm at pH 4, to 8.48 ppm at pH 8, with a pKa of approximately 4.5, where no other residues displayed significant chemical shifts for either their backbone amide or side chain resonances within this pH range.

[10] A well-defined type I β-turn spanning residues Asp^{134}-Glu-Gln-Phe^{137} and a well-defined type II β-turn spanning Pro^{139}-Lys-Gly-Cys^{142} are also present at pH 7.2, as identified by ^{1}H NMR structural studies of the synthetic PAK pilin peptide at this pH.

ing. Conformational exchange may therefore provide a mechanism for modulating available intrinsic binding energy, preserving moderate affinities for optimal biological function.

The relaxation measurements for the PAK pilin peptide presented here show slow motions on the μs–ms time scale for Thr^{130} near the disulfide bridge, and for Gln^{136}, Phe^{137}, Ile^{138} and Lys^{140} within the ordered β-turns, indicative of conformational exchange processes affecting these regions of the sequence. ^{1}H NMR-monitored titrations of the synthetic PAK pilin peptide with Mab PAK-13 (Campbell et al., 1997b) demonstrated significant linebroadening for backbone and side-chain resonances of residues within the turns or near the disulfide bridge. Thus, the most plastic regions of the sequence also appear to be the regions most immobilized upon antibody binding, consistent with the induced-fit model.

It is interesting that the site of the greatest conformational exchange (Ile^{138}) is found between the two turns, centered within the structural epitope proposed for antibody recognition. The existence of conformational exchange within the epitope region may affect the immunogenicity of the PAK pilin peptide in two different ways. First, conformational exchange may serve to increase the conformational entropy of the free state, thereby attenuating antibody affinities for optimal biological function. Secondly, conformational exchange may provide a mechanism for cross-reactivity of the same immunogen with different antibodies, or of the same antibody with different immunogens, thereby increasing the probability of humoral immune detection of pathogen. This mechanism may allow Mab PAK-13 to recognize and bind the intact pilin protein from several different strains of *P. aeruginosa.*

Backbone motions are an intrinsic component of PAK pilin immunogenicity. In order to further probe their role in immune recognition of the PAK pilin system, future studies by this group will include ^{15}N NMR relaxation measurements of the ^{15}N-labeled recombinant PAK pilin peptide bound to Mab PAK-13. These studies will allow a direct measurement of changes in the amplitude and frequencies of backbone motions of the PAK pilin peptide as a function of binding. This will allow changes in conformational entropy between the free and bound state to be approximated, and the role of conformational exchange in antibody recognition and binding to be addressed.

Significance with respect to peptide vaccine design

Since the β-turns in the pilin system have been implicated in antibody recognition (Campbell et al., 1997b), features designed to stabilize the turns should result in increased antibody affinity and enhanced immunogenicity. In fact, conformationally constraining peptide antigens in order to stabilize β-turns has been shown in practice to increase antibody affinity (Hinds et al., 1991; Blumenstein et al., 1992). However, design strategies which constrain a peptide immunogen into the desired conformation strive toward the 'lock-and-key' model of binding in which antibody affinity and specificity are presumably maximized. Were our goal to design a strain-specific PAK pilin peptide vaccine effective against *P. aeruginosa* strain K infections only, the next logical step might be the design of constrained PAK pilin peptide analogs or even peptidomimetics. However, our goal is cross-protection against a broad spectrum of *P. aeruginosa* strains, so design strategies must instead strive toward an induced-fit model, in which the dynamics of the free and bound states modulate binding energy and allow for cross-reactivity in recognition and binding. To this end, a detailed picture of the dynamics involved in antibody recognition of pilin immunogens is a necessary component of the vaccine design process, providing critically important information to the generation of an immune response effective against the multiple strains of *P. aeruginosa.*

Conclusions

The results presented here emphasize the importance of using both the model-free approach and spectral density mapping when interpreting ^{15}N NMR relaxation studies of flexible peptides in solution. The strengths of the model-free approach reside in its ability to extract quantitative measurements of correlation times and exchange rates, and in its ability to provide a satisfying picture of backbone motions. However, in the case of the recombinant PAK pilin peptide, the model-free formalism failed for temperatures greater than 5 °C, as the increased contribution of internal motions made the extraction of a global correlation time difficult. The strength of the spectral density mapping approach is that it makes no assumption as to the appropriate choice of motional model, and can be used to assess backbone dynamics even when the concept of a global correlation time is meaningless. In the case of the PAK pilin peptide, spectral density mapping al-

lowed for an analysis of the effects of temperature on backbone dynamics.

The results presented here also emphasize the importance of acquiring relaxation data at multiple fields, multiple temperatures, and even multiple pH. In the case of the PAK pilin peptide, this approach allowed the qualitative assessment of slow time-scale conformational exchange processes affecting different regions in the sequence, processes that are likely to play a key role in determining the binding affinity of the PAK pilin peptide.

Acknowledgements

The authors would like to thank Stéphane Gagné for NMR assistance with the ^{15}N relaxation pulse sequences, and Robert Boyko and Leigh Willard for computer programming assistance. This work was funded by the Protein Engineering Network of Centres of Excellence (PENCE), and the Canadian Bacterial Diseases Network (CBDN), which are both funded by the Government of Canada.

References

Akke, M., Skelton, J.H., Kordel, J., Palmer, A.G. and Chazin, W.J. (1993) *Biochemistry*, **32**, 9832–9844.

Alexandrescu, A.T., Rathgeb-Szabo, K., Rumpel, K., Jahnke, W., Schulthess, T. and Kammerer, R.A. (1998) *Protein Sci.*, **7**, 389–402.

Bai, Y., Milne, J.S., Mayne, L. and Englander, S.W. (1993) *Proteins*, **17**, 75–86.

Barbar, E., Hare, M., Daragan, V., Barany, G. and Woodward, C. (1998) *Biochemistry*, **37**, 7822–7833.

Barbato, G., Ikura, M., Kay, L.E., Pastor, R.W. and Bax, A. (1992) *Biochemistry*, **31**, 5269–5278.

Beeser, S.A., Oas, T.G. and Goldenberg, D.P. (1998) *J. Mol. Biol.*, **284**, 1581–1596.

Beglova, N., LeSauteur, L., Ekiel, I., Saragovi, H.U. and Gehring, K. (1998) *J. Biol. Chem.*, **273**, 23652–23658.

Blackledge, M.J., Brüschweiler, R., Griesinger, C., Schmidt, J.M., Xu, P. and Ernst, R.R. (1993) *Biochemistry*, **32**, 10960–10974.

Blumenstein, M., Matsueda, G.R., Timmons, S. and Hawiger, J. (1992) *Biochemistry*, **31**, 10692–10698.

Briand, J. and Kopple, K.D. (1995) *J. Biomol. NMR*, **6**, 347–360.

Campbell, A.P., McInnes, C., Hodges, R.S. and Sykes, B.D. (1995) *Biochemistry*, **34**, 16255–16268.

Campbell, A.P., Bautista, D.L., Tripet, B., Irvin, R.T., Hodges, R.S. and Sykes, B.D. (1997a) *Biochemistry*, **36**, 12791–12801.

Campbell, A.P., Wong, W.Y., Houston Jr., M.E., Schweizer, F., Cachia, P.J., Irvin, R.T., Hindsgaul, O., Hodges, R.S. and Sykes, B.D. (1997b) *J. Mol. Biol.*, **267**, 382–402.

Campbell, A.P., Wong, W.Y., Irvin, R.T. and Sykes, B.D. (2000) manuscript submitted to *Biochemistry*.

Chen, C., Feng, Y., Short, J.H. and Wand, J. (1993) *Arch. Biochem. Biophys.*, **306**, 510–514.

Clore, G.M., Szabo, A., Bax, A., Kay, L.E., Driscoll, P.C. and Gronenborn, A.M. (1990) *J. Am. Chem. Soc.*, **112**, 4989–4992.

Crump, M.P., Spyracopoulos, L., Lavigne, P., Kim, K.-S., Clark-Lewis, I. and Sykes, B.D. (1999) *Protein Sci.*, **8**, 2041–2054.

Daragan, V.A., Ilyina, E.E., Fields, C.G., Fields, G.B. and Mayo, K.H. (1997) *Protein Sci.*, **6**, 355–363.

Davis, J.H., Agard, D.A., Handel, T.M. and Basus, V.J. (1997) *J. Biomol. NMR*, **10**, 21–27.

Davis, J.H. and Agard, D.A. (1998) *Biochemistry*, **37**, 7696–7707.

Delaglio, F., Grzesiek, S., Vuister, G.W., Zhu, G., Pfeifer, J. and Bax, A. (1995) *J. Biomol. NMR*, **6**, 277–293.

Dellwo, M.J. and Wand, A.J. (1989) *J. Am. Chem. Soc.*, **111**, 4571–4578.

Englander, J.J., Calhoun, D.B. and Englander, S.W. (1979) *Anal. Biochem.*, **92**, 517–524.

Englander, S.W. and Kallenbach, N.R. (1984) *Q. Rev. Biophys.*, **16**, 521–655.

Epstein, D.M., Benkovic, S.J. and Wright, P.E. (1995) *Biochemistry*, **34**, 11037–11048.

Fan, P., Li, M.-H., Brodsky, B. and Baum, J. (1993) *Biochemistry*, **32**, 13299–13309.

Fan, P. and Mayo, K.H. (1995) *J. Biol. Chem.*, **270**, 24693–24701.

Farrow, N.A., Muhandiram, R., Singer, A.U., Pascal, S.M., Kay, C.M., Gish, G., Shoelson, S.E., Pawson, R., Forman-Kay, J.D. and Kay, L.E. (1994) *Biochemistry*, **33**, 5984–6003.

Farrow, N.A., Zhang, O., Szabo, A., Torchia, D.A. and Kay, L.E. (1995) *J. Biomol. NMR*, **6**, 153–162.

Friedrichs, M.S., Stouch, T.R., Bruccoleri, R.E., Mueller, L. and Constantine, K.L. (1995) *J. Am. Chem. Soc.*, **117**, 10855–10864.

Garrett, D.S., Powers, R., Gronenborn, A.M. and Clore, G.M. (1991) *J. Magn. Reson.*, **95**, 214–220.

Grathwohl, C. and Wüthrich, K. (1981) *Biopolymers*, **20**, 2623–2633.

Grzesiek, S. and Bax, A. (1993a) *J. Biomol. NMR*, **3**, 627–638.

Grzesiek, S. and Bax, A. (1993b) *J. Am. Chem. Soc.*, **115**, 12593–12594.

Hinds, H.G., Welsh, J.H., Brennand, D.M., Fisher, J., Glennie, M.J., Richards, H.G.J., Turner, D.L. and Robinson, J.A. (1991) *J. Med. Chem.*, **34**, 1777–1789.

Hu, Y., MacInnes, J.M., Cherayil, B.J., Fleming, G.R., Freed, K. and Perico, A. (1990) *J. Chem. Phys.*, **93**, 822–826.

Hyre, D.E. and Klevit, R.E. (1998) *J. Mol. Biol.*, **279**, 929–943.

Ikura, M., Kay, L.E., Krinks, M. and Bax, A. (1991) *Biochemistry*, **30**, 5498–5504.

Jarvis, A.J. and Craik, D.J. (1995) *J. Magn. Reson.*, **B107**, 95–106.

Kay, L.E. (1998) *Nat. Struct. Biol.*, **5** (Suppl), 513–517.

Kemple, M.D., Buckley, P., Yuan, P. and Prendergast, F.G. (1997) *Biochemistry*, **36**, 1678–1688.

Kontaxis, G., Konrat, R., Krautler, B., Weiskirchen, T. and Bister, K. (1998) *Biochemistry*, **37**, 7127–7134.

Kopple, K.D., Wang, Y.-S., Cheng, A.G. and Bhandary, K.K. (1988) *J. Am. Chem. Soc.*, **110**, 4168–4176.

Li, Y.C. and Montelione, G.T. (1995) *Biochemistry*, **34**, 2408–2423.

Lipari, G. and Szabo, A. (1982a) *J. Am. Chem. Soc.*, **104**, 4546–4559.

Lipari, G. and Szabo, A. (1982b) *J. Am. Chem. Soc.*, **104**, 4559–4570.

LiWang, A.C., Cao, J.J., Zheng, H., Lu, Z., Peiper, S.C. and LiWang, P.J. (1999) *Biochemistry*, **38**, 442–453.

Lu, J. and Van Halbeek, H. (1997) *Biophys. J.*, **72**, 470–481.

Mandel, A.M., Akke, M. and Palmer, A.G. (1996) *Biochemistry*, **35**, 16009–16023.

McInnes, C., Kay, C.M., Hodges, R.S. and Sykes, B.D. (1994) *Biopolymers*, **34**, 1221–1230.

Mikhailov, D., Mayo, K.H., Pervin, A. and Linhardt, R.J. (1996) *Biochem. J.*, **315**, 447–454.
Nall, B.T. and Zuniga, E.H. (1990) *Biochemistry*, **29**, 7576–7584.
Nicholson, L.K., Kay, L.E., Baldisseri, D.M., Arango, J., Young, P.E., Bax, A. and Torchia, D.A. (1992) *Biochemistry*, **31**, 5253–5263.
Nicholson, L.K., Yamazaki, T., Torchia, D.A., Grzesiek, S., Bax, A., Stahl, S.J., Kaufman, J.D., Wingfield, P.T., Lam, P.Y., Jadhav, P.K. et al. (1995) *Nat. Struct. Biol.*, **2**, 274–280.
Otting, G., Liepinsch, E. and Wüthrich, K. (1993) *Biochemistry*, **32**, 3571–3582.
Palmer, A.G., Rance, M. and Wright, P.E. (1991) *J. Am. Chem. Soc.*, **113**, 4371–4380.
Palmer, A.G. and Case, D.A. (1992) *J. Am. Chem. Soc.*, **114**, 9059–9067.
Palmer, A.G., Hochstrasser, R.A., Millar, D.P., Rance, M. and Wright, P.E. (1993) *J. Am. Chem. Soc.*, **115**, 6333–6345.
Palmer, A.G. (1997) *Curr. Opin. Struct. Biol.*, **7**, 732–737.
Peng, J.W. and Wagner, G. (1992a) *Biochemistry*, **31**, 8571–8586.
Peng, J.W. and Wagner, G. (1992b) *J. Magn. Reson.*, **98**, 308–332.
Roberts, G.C.K. (1999) *Curr. Opin. Biotechnol.*, **10**, 42–47.
Shaka, A.J., Keeler, J., Frenkiel, T. and Freeman, R. (1983) *J. Magn. Reson.*, **52**, 335–338.
Sheth, H.B., Glasier, L.M.G., Ellert, N.W., Cachia, P., Kohn, W., Lee, K.K., Paranchych, W., Hodges, R.S. and Irvin, R.T. (1995) *Biomed. Pept., Proteins Nucleic Acids*, **1**, 141–148.
Skelton, N.J., Palmer, A.G., Akke, M., Kördel, J., Rance, M. and Chazin, W.J. (1993) *J. Magn. Reson.*, **B102**, 253–264.
Sørensen, M.D., Bjørn, S., Norris, K., Olsen, O., Petersen, L., James, T.L. and Led, J.J. (1997) *Biochemistry*, **36**, 10439–10459.
Spyracopoulos, L., Yee, A.A. and O'Neil, J.D.J. (1996) *J. Biomol. NMR*, **7**, 283–294.
Stivers, J.T., Abeygunawardana, C. and Mildvan, A.S. (1996) *Biochemistry*, **35**, 16036–16047.
Szyperski, T., Luginbühl, P., Otting, G., Güntert, P. and Wüthrich, K. (1993) *J. Biomol. NMR*, **3**, 151–164.
Tripet, B., Yu, L., Bautista, D.L., Wong, W.Y., Irvin, R.T. and Hodges, R.S. (1996) *Protein Eng.*, **9**, 1029–1042.
Wagner, G., Bruhwiler, D. and Wüthrich, K. (1987) *J. Mol. Biol.*, **196**, 227–331.
Wong, W.Y., Campbell, A.P., McInnes, C., Sykes, B.D., Paranchych, W., Irvin, R.T. and Hodges, R.S. (1995) *Biochemistry*, **34**, 12963–12972.
Zidek, L., Novotny, M.V. and Stone, M.J. (1999) *Nat. Struct. Biol.*, **6**, 1118–1121.
Zinn-Justin, S., Berthault, P., Guenneugues, M. and Desvaux, H. (1997) *J. Biomol. NMR*, **10**, 363–372.